Received: 30 September 2022 | Accepted: 21 December 2022

DOI: 10.1002/pamm.202200048

Numerical simulation of the thermal wave induced by a moving interfacial heat source with respect to Christov–Cattaneo's equation

Marvin C. Feike[1,*] and **Christian Mundt**[1]

[1] Institute of Thermodynamics, Universität der Bundeswehr München, Neubiberg, Germany

The hyperbolic wave equation of heat conduction with respect to Christov's formulation is utilized with the Streamline-Upwind-Petrov-Galerkin method in space and the Θ, Houbolt, linear acceleration, Wilson-Θ and Newmark methods in time. The derivation of this equation and its matrix formulation are shown. A 2D transient finite element simulation of a generic asperity with an infinite line heat source in an interface, either as a heat flux density $\dot{q}$ or temperature distribution T, is performed for $\mathrm{Ma}_{\mathrm{th}} = [0.5; 1.0]$. A sensitivity study is presented for the mentioned numerical schemes. The temperature jump in the solution is interpreted as an indicator for a thermal shock.

1 Introduction

Frictional contact between two solid bodies can be modeled as the thermal effect of a moving heat source at their interfaces. This contact affects the thermal distribution. Specifically, on short time scales, the partitioning of the heat flux and the propagation of the transient temperature field are of interest. Both depend on geometrical boundary conditions, the material properties, and the relative velocity. The latter two determine the time scale. If the physical time scale is nanoseconds or shorter, e.g. as for metals, then the heat transport can be modeled by the hyperbolic heat equation rather than the parabolic Fourier equation. This is, because the heat propagation is considered in form of thermal waves in a non-equilibrium state. One approach is to use Christov-Cattaneo's hyperbolic equation (CC) by Christov [1] to determine thermodynamic effects. Moreover, if the moving heat source is as fast or faster than the thermal wave, a thermal shock is expected near the moving heat source during the transient process.

The hyperbolic heat conduction equation by Christov-Cattaneo is simulated for a contact problem in a moving frame of reference for a relative velocity near thermal wave speed. The current work expands on recent results for the CV equation from Feike [2], by considering the CC equation and additional time integration schemes. The implicit time-marching of the θ, Houbolt, linear acceleration, Wilson-θ and Newmark methods are now considered in addition to the spatial discretization by the Galerkin finite element method. Finally, numerical simulations of an asperity as intermediate contact of two bodies in relative movement to each other are performed. The line heat source, a consequence of this frictional contact, is modeled either as a heat flux or a temperature distribution in this interface.

2 Heat transport with respect to Christov-Cattaneo's equation

Important applications for the hyperbolic heat equation are discussed by Joseph [3], Lebon [4], Tzou [5, 6] and Nosko [7]. Additional advancements are made by Christov [1], who correct the Maxwell-Cattaneo (MC) law of finite-speed heat conduction. The MC law and the CV approach only differ in the notation of the relaxation parameter, but not in the physical meaning of the heat transport. Therefore, Christov's suggestion to use the material derivative in the moving body can be applied to the CV equation which also leads to the CC formulation. The CC hyperbolic heat transport equation is derived by assembling the balance equation for the internal energy with Christov's assumption for heat conduction. The balance and heat equation are formulated in the material frame.

The balance law for the internal energy has the form (e.g. [8]), with the density ρ, specific heat capacity c, temperature T, time t, heat flux density $\dot{\boldsymbol{q}}$ and volumetric heat source $\dot{q}_V$:

$$\rho c \frac{DT}{Dt} + \nabla \cdot \dot{\boldsymbol{q}} + \dot{q}_V = 0. \tag{1}$$

Christov points out the need of the material derivative in the MC law for a body in motion. This is now assumed for the CV equation, where the partial time derivative of the heat flux density is substituted by the material derivative. With the relaxation time τ and heat conduction λ, the Christov's form is:

$$\tau \frac{D\dot{\boldsymbol{q}}}{Dt} + \dot{\boldsymbol{q}} = -\lambda \nabla T. \tag{2}$$

* Corresponding author: marvin.feike@unibw.de

Rearranging equation (2) and substituting $\dot{\boldsymbol{q}}$ into (1) results in the PDE for the heat transport with respect to Christov-Cattaneo's equation. For simplifications, the volumetric heat source $\dot{q}_V$ is neglected and an anisotropic heat conduction λ plus constant system velocity $\boldsymbol{v}$ is set.

$$\rho c\big(\tau T_{tt} + 2\tau(\boldsymbol{v}\cdot\nabla T)_t + T_t + \tau(\boldsymbol{v}\cdot\nabla)^2 T + \boldsymbol{v}\cdot T\big) = \lambda\nabla^2 T \tag{3}$$

Equation (3) defines the finite propagation speed of the thermal wave in a moving frame of reference. This speed is the sum of the thermal wave velocity C, which is assumed to be isotropic, see Tzou [9], and the system or heat source speed in the interface $\boldsymbol{v}$. A thermal Mach number $\mathrm{Ma_{th}}$ can be defined as the ratio of the speed of the movement $\boldsymbol{v}$ and thermal wave C. According to Gómez [10], the ranges of the Mach number can be named:

$$\begin{aligned}
&\boldsymbol{c} = C \pm \boldsymbol{v} = \sqrt{\frac{\alpha}{\tau}} \pm \boldsymbol{v} \ \text{ and } \ \mathrm{Ma_{th}} = \frac{\boldsymbol{v}}{C}, \ \text{ with}\\
&\mathrm{Ma_{th}} < 1 \rightarrow \text{Subsonic resp. subcritical diffusion,}\\
&\mathrm{Ma_{th}} = 1 \rightarrow \text{Transonic resp. transcritical diffusion,}\\
&\mathrm{Ma_{th}} > 1 \rightarrow \text{Supersonic resp. supercritical diffusion.}
\end{aligned} \tag{4}$$

The boundary conditions used for the simulation domain are Dirichlet, Neumann and Robin (e.g. [11]). In the contact surface, a semi-infinite line heat source is set with a constant heat flux density $\dot{q}$ and a constant temperature T. For simplification, those values are not varied over the length of the heat source, or in time.

3 Numerical methods

3.1 Spatial integration: Streamline-Upwind-Petrov-Galerkin-FEM

To simulate and investigate the thermal wave, equation (3) has to be transformed into a numerically solvable form. To do so for a frictional contact problem of solid bodies, the widely used finite element formulation of the Galerkin weighted residual method (GFEM) is applied. The use of the GFEM leads to a weak form, where the second-order spatial derivatives have to be integrated using the Green-Gauss divergence theorem. The GFEM approach leads to an unstable solution for the CC equation. Recent work by Feike [2] applies the Streamline-Upwind-Petrov-Galerkin-FEM (SUPG) to the CV equation. This method will be used here once more, because advection dominated transport problems lead to numerical instabilities and an upwind scheme is known to stabilize the simulation (e.g. [12], [13]). The SUPG formulation of the hyperbolic heat conduction equation with respect to the Christov-Cattaneo equation for a finite element, with its shape function N^e integrated over the element domain Ω^e and boundary integral Γ^e, is:

$$\begin{aligned}
&\underbrace{\int_{\Omega^e} N^e \rho c\big(\tau T_{tt} + \ 2\tau(\boldsymbol{v}\cdot\nabla T)_t + T_t + (\boldsymbol{v}\cdot\nabla)T\big) d\Omega^e}_{\text{Systems inertia and partly stiffness}} - \underbrace{\int_{\Omega^e} \rho c\tau(\boldsymbol{v}\cdot\nabla N^e, \boldsymbol{v}\cdot\nabla T)\, d\Omega^e}_{\text{Natural diffusion inside the domain}}\\
&+ \underbrace{\int_{\Gamma^e} \rho c\tau\big((\boldsymbol{v}\cdot\boldsymbol{n})N^e, \boldsymbol{v}\cdot\nabla T\big) d\Gamma^e}_{\text{Natural diffusion on the boundary}} + \underbrace{\int_{\Omega^e} \lambda\nabla N^e\cdot\nabla T d\Omega^e}_{\text{Fourier's diffusion}} + \underbrace{\int_{\Omega^e} P(N^e)\gamma R d\Omega^e}_{\text{Stabilization term, artificial diffusion}} = \underbrace{\int_{\Gamma^e} N^e(\mathrm{BC}) d\Gamma^e}_{\text{Boundary conditions}}.
\end{aligned} \tag{5}$$

The first integral in equation (5) represents the system inertia with its time derivatives, but also contains a part of the system's stiffness. More over, the next diffusion terms occur additional to the Fourier's diffusion, where the first and second are natural and the last originates as artificial diffusion from the SUPG. The two natural terms result from the weak formulation, where on the boundary it is necessary to counteract spurious reflections, see [14]. The second integral in the equation is a natural term representing diffusivity and is similar to the artificial diffusion term of the SUPG stabilization. This is due the assumption of time-independent shape functions for the perturbation coefficient $P(N^e)$ and thus reduces to an advection term, see Bochev [15]:

$$P(N^e) = \frac{DN^e}{Dt} = \frac{\cancelto{0}{dN^e}}{\cancel{\Delta t}} + \boldsymbol{v}\cdot\nabla N^e = \boldsymbol{v}B^e. \tag{6}$$

A good choice for the stabilization parameter γ in the stabilization term is mentioned by Donea [12]. He and et al. suggest

$$\gamma = \frac{\bar{\alpha}}{2||\boldsymbol{v}||^2}\frac{1}{\Theta}, \ \text{with } \bar{\alpha} = \beta\frac{\boldsymbol{v}L}{2} = \beta\alpha\mathrm{Pe}, \ \beta = coth(\mathrm{Pe}) - \frac{1}{\mathrm{Pe}} \ \text{and } \mathrm{Pe} = \frac{\boldsymbol{v}L}{2\alpha}, \tag{7}$$

for advection dominant problems (with $\Theta = 1/2$ in the present case). Here $\bar{\alpha}$ is the unknown artificial diffusion, L the characteristic element length and Pe the element Peclet number. The dependence of γ on several variables, like the material

property α and mesh properties L and velocity $\boldsymbol{v}$, is clearly shown and must be calculated individually. Selecting γ for the present case is restricted by equation (7). The residual R is the hyperbolic equation by itself, where the diffusion term can be neglected, see Huang [16]. With that reduction, and equations (6) and (7), the stabilization term becomes

$$\int_{\Omega^e} P(N^e)\gamma R d\Omega^e = \int_{\Omega^e} \boldsymbol{v} B^e \gamma \left(\rho c \left(\tau T_{tt} + 2\tau(\boldsymbol{v}\cdot\nabla T)_t + T_t + \tau(\boldsymbol{v}\cdot\nabla)^2 T + \boldsymbol{v}\cdot T \right) \right) d\Omega^e. \tag{8}$$

Hint: the diffusion term $\int_{\Omega^e} \rho c \tau (\boldsymbol{v}\cdot\nabla)^2 T d\Omega^e$ must be integrated by the Green-Gauss divergence theorem to linearize, otherwise the term vanishes for linear elements. The last term in equation (5) is a boundary integral, which sets the boundary conditions BC for the domain.

3.2 Time discretization: Θ, Houbolt, linear acceleration, Wilson-Θ and Newmark methods

Multiple time-marching schemes are considered to compare their behavior. This includes the direct integration forms of Θ, Houbolt, linear acceleration and its evolved Wilson-Θ and Newmark methods. To cast the hyperbolic heat transport equation in (5) in a convenient form, the global matrix and vector formulation is used, with the mass matrix $\mathbf{M}$, stiffness matrices $\mathbf{K}_{\boldsymbol{v}}$, $\mathbf{K}_{\mathrm{D}}$, $\mathbf{K}_{\lambda,h}$, stiffness vector $\boldsymbol{k}_{\mathrm{D}}$ and force vector $\boldsymbol{f}$:

$$\tau\mathbf{M}\ddot{T} + (\mathbf{M} + 2\tau\mathbf{K}_{\boldsymbol{v}})\dot{T} + (\mathbf{K}_{\boldsymbol{v}} + \mathbf{K}_{\lambda,h} - \tau\mathbf{K}_{\mathrm{D}} + \tau\boldsymbol{k}_{\mathrm{D}})T = \boldsymbol{f}. \tag{9}$$

Equation (9) has now the identical structure to a mechanical finite element system in motion. Where $\mathbf{M}^*$, $\mathbf{C}^*$, $\mathbf{K}^*$, and $\mathbf{R}^*$ can be set as mass, stiffness, and damping matrices, and external load vector:

$$\begin{aligned} &\mathbf{M}^*\ddot{T} + \mathbf{C}^*\dot{T} + \mathbf{K}^* T = \mathbf{R}^* \ \text{ with} \\ &\mathbf{M}^* := \tau\mathbf{M}, \ \ \mathbf{C}^* := \mathbf{M} + 2\tau\mathbf{K}_{\boldsymbol{v}}, \ \ \mathbf{K}^* := \mathbf{K}_{\boldsymbol{v}} + \mathbf{K}_{\lambda,h} - \tau\mathbf{K}_{\mathrm{D}} + \tau\boldsymbol{k}_{\mathrm{D}}, \ \text{ and } \ \mathbf{R}^* := \boldsymbol{f}. \end{aligned} \tag{10}$$

With equation (10) and the formulation of a linear system with $\mathbf{A}T = \boldsymbol{b}$, it is straightforward to utilize the time integration schemes and set up the algorithms at the time steps $n-1$, n and $n+1$. The Θ method is shown by Huebner [13], with e.g. $\Theta = 1/2$ it is the common implicit Crank-Nicolson scheme:

$$\begin{aligned} &\mathbf{A} = a_0\mathbf{M}^* + a_1\mathbf{C}^* + \Theta\mathbf{K}^* \ \text{ and} \\ &\boldsymbol{b} = \Theta\mathbf{R}^{*n+1} + (1-\Theta)\mathbf{R}^{*n} + \mathbf{M}^*(-a_0 T^{n-1} + a_2 T^n) + \mathbf{C}^* a_1 T^n - (1-\Theta)\mathbf{K}^* T^n, \ \text{ with} \\ &a_0 = \frac{1}{\Delta t^2}, a_1 = \frac{1}{\Delta t} \ \text{ and } \ a_2 = 2a_0. \end{aligned} \tag{11}$$

The Houbolt method from Bathe [17] is

$$\begin{aligned} &\mathbf{A} = \mathbf{K}^* + a_0\mathbf{M}^* + a_1\mathbf{C}^* \ \text{ and} \\ &\boldsymbol{b} = \mathbf{R}^{*n+1} + \mathbf{M}^*(a_2 T^n + a_4 T^{n-1} + a_6 T^{n-2}) + \mathbf{C}^*(a_3 T^n + a_5 T^{n-1} + a_7 T^{n-2}) \ \text{ with} \\ &a_0 = \frac{2}{\Delta t^2}, a_1 = \frac{11}{6\Delta t}, a_2 = \frac{5}{\Delta t^2}, a_3 = \frac{3}{\Delta t}, a_4 = -2a_0, a_5 = \frac{-a_3}{2}, a_6 = \frac{a_0}{2} \ \text{ and } \ a_7 = \frac{a_3}{9}. \end{aligned} \tag{12}$$

In addition to the two schemes mentioned, similar integrations of Wilson-Θ [17] and the linear acceleration method [18] are also considered. The Wilson-Θ method (with $\Theta = 1.4$ in the present case) is an extended version of the linear acceleration method (with $\Theta = 1$):

$$\begin{aligned} &\mathbf{A} = \mathbf{K}^* + a_0\mathbf{M}^* + a_1\mathbf{C}^* \ \text{ and} \\ &b = \mathbf{R}^{*n} + \Theta(\mathbf{R}^{*n+1} - \mathbf{R}^{*n}) + \mathbf{M}^*(a_0 T^n + a_2\dot{T}^n + 2\ddot{T}^n) + \mathbf{C}^*(a_1 T^n + 2\dot{T}^n + a_3\ddot{T}^n) \ \text{ with} \\ &a_0 = \frac{6}{(\Theta\Delta t)^2}, a_1 = \frac{3}{\Theta\Delta t}, a_2 = 2a_1, a_3 = \frac{\Theta\Delta t}{2}, a_4 = \frac{a_0}{\Theta}, a_5 = \frac{-a_2}{\Theta}, a_6 = 1 - \frac{3}{\Theta}, a_7 = \frac{\Delta t}{6} \ \text{ and } \ a_8 = \frac{\Delta t^2}{6}. \end{aligned} \tag{13}$$

The final time stepping scheme is the Newmark method [18]. Here the parameter $\delta = 0.75$ and $\alpha = 0.25\,(0.5+\delta)^2 = 0.39$ are proposed by the investigations of Rostami [19]:

$$\begin{aligned} &\mathbf{A} = \mathbf{K}^* + a_0\mathbf{M}^* + a_1\mathbf{C}^* \ \text{ and} \\ &b = \mathbf{R}^{*n+1} + \mathbf{M}^*(a_0 T^n + a_2\dot{T}^n + a_3\ddot{T}^n) + \mathbf{C}^*(a_1 T^n + a_4\dot{T}^n + a_5\ddot{T}^n) \ \text{ with} \\ &a_0 = \frac{1}{\alpha t^2}, a_1 = \frac{\delta}{\alpha\Delta t}, a_2 = \frac{1}{\alpha\Delta t}, a_3 = \frac{1}{2\alpha} - 1, a_4 = \frac{\delta}{\alpha} - 1, a_5 = \frac{\Delta t}{2}\left(\frac{\delta}{\alpha} - 2\right), a_6 = \Delta t(1-\delta), a_7 = \delta\Delta t. \end{aligned} \tag{14}$$

4 Simulation of a generic asperity

The present problem is a generic asperity between two solid bodies as an intermediate frictional contact domain. The rubbing process is modeled as a 1D semi-infinite line heat source with either a heat flux or a temperature distribution. For simplification it is assumed, that all energy is transformed into heat. It is of interest if an asymmetrical temperature field in the contact region will build up and if a thermal wave is induced. In addition, numerical investigations on the time integration schemes and of three mesh refinements are performed.

4.1 Numerical setup

Figure 1 shows the contact between solid body 1 (in motion with speed $\boldsymbol{v}$) and the asperity of solid body 2 (in rest). For completeness, the material properties and boundary conditions on the edges to the ambient and far-field are shown. To start with the material properties, both bodies are made of steel with the same λ, ρ, c and τ. The 2D relaxation time τ was determined as in Tzou [9]. The two cases of the semi-infinity line heat source are first set to $\dot{q}_\mathrm{n} = \dot{q}\, L_\mathrm{coarse}/(\lambda\, T_\infty) = 1 \times 10^{-1}$ and then, for the temperature BC, to a constant temperature of $T = 2\, T_\infty$. Furthermore, a Robin BC with the heat flux $\dot{q}_{n,\infty} = T_\infty\, h/\dot{q} = 1 \times 10^{-4}$ is applied to the inner boundary edges, and all other hatched edges use the adiabatic Neumann BC. The velocity $\boldsymbol{v}$ is limited in x_n-direction with v_x and set to two different values, depending on $\mathrm{Ma}_\mathrm{th} = [0.5; 1.0]$, see equation (4). The discretization is carried out with linear Lagrangian quadrilateral elements, where a mesh refinement study with respect to the normalized element length L_n in table 1 is performed. To resolve the wave properly, the element length L is smaller than the wave distance $C\tau$ and the time marching size will be $\Delta t < \tau$. The system of equations is solved with a LU preconditioning. To compare the time integration schemes, one monitoring point (MP) is defined below the heat source line.

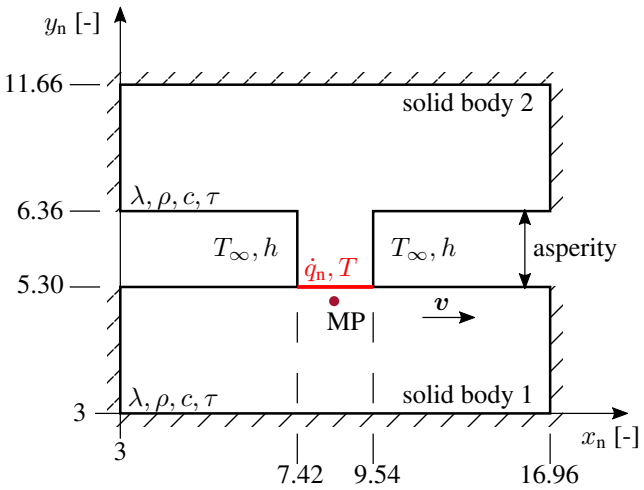

Fig. 1: Problem domain of asperity and its boundary conditions.

Table 1: Parameters of the mesh refinement study.

Mesh	Number of nodes	$L_\mathrm{n} = L/(C\,\tau)$
coarse	16200	0.1060
medium	64800	0.0530
fine	259200	0.02565

4.2 Temperature profiles with the line heat source types: $\dot{q}_\mathrm{n}$ and T

The 2D solutions at time τ of the temperature T_n distribution, which is normalized by the maximal temperature, are shown in figures 2 to 5, where the Θ method of Crank-Nicolson and a fine mesh are used. Four states are depicted, where two different kinds of line heat sources ($\dot{q}_\mathrm{n}, T$), and different thermal Mach numbers $\mathrm{Ma}_\mathrm{th} = [0, 5; 1, 0]$ are considered. In general, all solutions show the correct physical behavior of an antisymmetric temperature profile, which is moved downstream in the x_n-direction in body 1, see Kennedy in [20]. Upstream, the temperature profile propagates slower for $\mathrm{Ma}_\mathrm{th} = 0.5$, which is the result of the relative velocity as the difference of the system speed $\boldsymbol{v}$ minus the heat wave propagation speed C, see equation (4). Zero upstream propagation is pictured for $\mathrm{Ma}_\mathrm{th} = 1.0$, where the wave front is 'stuck' at the heat source leading edge ($x_\mathrm{n} = 7.42, y_\mathrm{n} = 5.30$), and a temperature jump due to a thermal shock is assumed. This shock front is seen in figure 3 and especially for the temperature BC in figure 5. For the latter one, the first nodes are near the front, which helps to get a more defined temperature jump. However, figure 4 and figure 5 feature a poor numerical solution in the contact surface, which is caused by the temperature BC acting as hard BC of first type. Moreover, a mesh dependency in this primary zone of heat generation was found. The coarser elements alleviate this problem, but generates a inaccurate solution in the far-field. To counteract that, the mesh can be refined from the far-field towards the heat source. In y_n, all cases are fairly independent of Ma_th for the temperature propagation and have a defined wave front traveling normal to the contact area. This front is more distinct in figures 4 and 5, due to the larger temperature gradient in the contact area. For $\dot{q}_\mathrm{n}$ in figure 2 and 3, the gradient is smoother in space. In general, the more realistic case will be the $\dot{q}_\mathrm{n}$ BC, with a heat source at the surface, as a consequence of the mechanical frictional contact. Also, the transient solution shows natural inert behavior, because the diffusion in form of the wave needs a certain amount of time. The second test case with T in the contact area enforces the thermal wave more, but shows a questionable temperature drop in the center and a rise on the leading edge, caused by numerical issues.

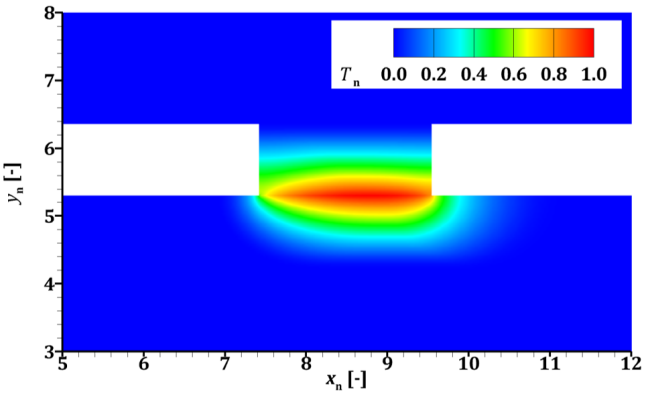

Fig. 2: T_n field with BC $\dot{q}_\mathrm{n}$ at time τ for $\mathrm{Ma}_\mathrm{th} = 0.5$.

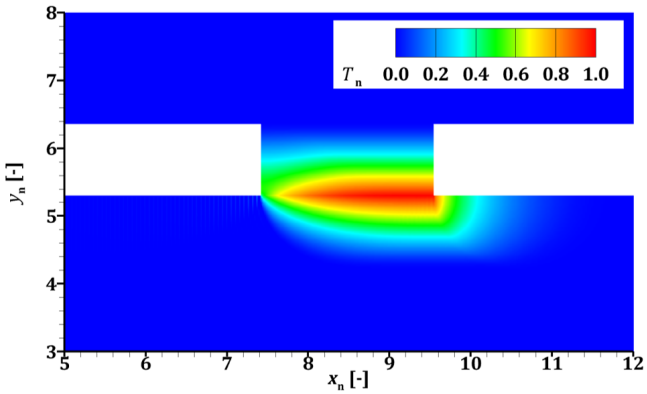

Fig. 3: T_n field with BC $\dot{q}_\mathrm{n}$ at time τ for $\mathrm{Ma}_\mathrm{th} = 1$.

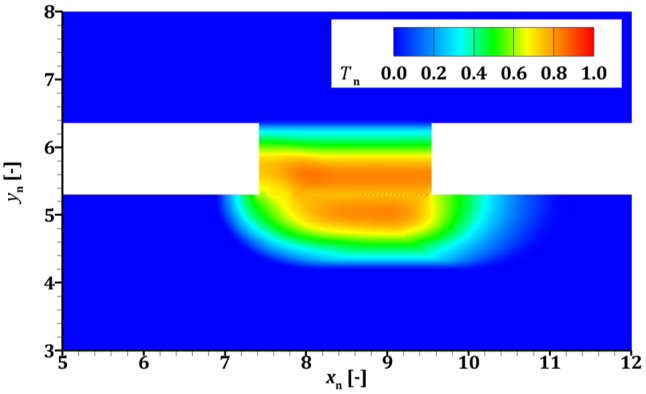

Fig. 4: T_n field with BC T at time τ for $\mathrm{Ma}_\mathrm{th} = 0.5$.

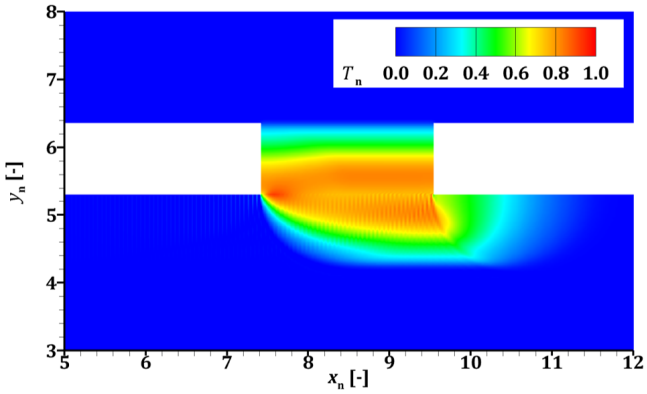

Fig. 5: T_n field with BC T at time τ for $\mathrm{Ma}_\mathrm{th} = 1$.

4.3 Time integration schemes: Θ, Houbolt, linear acceleration, Wilson-Θ and Newmark methods

The transient temperature evolution T_n of the monitoring point (see figure 1) for different time marching schemes and for the fine mesh are shown in figure 6. The embedded plot illustrates the transient evolution and the large one shows more details, when the wave hits the monitoring point. To start with, the solution for the line heat source $\dot{q}_\mathrm{n}$ (solid line) is stable for all time integration methods and does not vary. The scheme with the shortest computation time is the linear acceleration, where the slowest is the Θ method with about 25.7 % more time consumption, see table 2. A different behavior emerges for the temperature distribution as heat source BC (dashed line). All solutions feature a jump and wiggle towards the stationary solution (embedded plot). Let's take a closer look at $s = 10$, where the wave front hits the monitoring point. Here the Θ method is the most stablest and most damped one and it shows the smallest temperature drop. In contrast, it takes the longest computational time (about 5.06 % more than Houbolt). The stability of the Θ method can be derived from its numerical discretization scheme, with its consideration of the stiffness matrix $\mathbf{K}^*$ for the time step n in equation (11) and respectively in vector $\boldsymbol{b}$. This is in contrast with the peaks of the other schemes, especially the Wilson-Θ method, with the highest nonphysical temperature drop. In general the Θ method gives qualitatively the best solutions, while Houbolt's method has the lowest runtime.

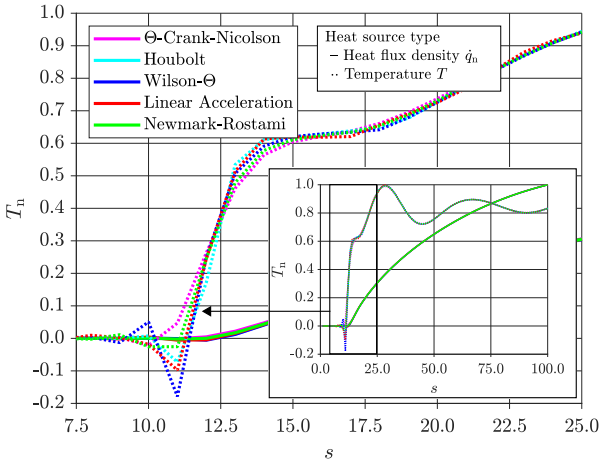

Fig. 6: T_n at $\mathrm{Ma}_\mathrm{th} = 1$ with fine mesh.

Table 2: Relative duration of numerical calculation times.

	Heat source type	
Scheme	Duration $\dot{q}_\mathrm{n}$	Duration T
Θ-Crank-Nicolson	25.7 %	5.06 %
Houbolt	0.35 %	0.00 %
Wilson-Θ	18.6 %	2.81 %
Linear Acceleration	0.00 %	4.03 %
Newmark-Rostami	1.38 %	0.11 %

4.4 Mesh refinement study

Figure 7 shows the transient convergence behavior of the numerical solution for the two heat source types and for three different mesh resolutions, see table 1. The data in figure 7 of the monitoring point MP (see figure 1) points out, that the best solution is achieved with the fine mesh. At the specific point $s = 10$, when the wave hits the monitoring point, and for both heat source types $\dot{q}_\mathrm{n}$ and T, the temperature of the coarse and medium mesh drops significantly to negative values, which is nonphysical. Then the temperature rise is smooth for the heat source $\dot{q}_\mathrm{n}$ case (solid line) and similar for its refinements. This is in contrast to the heat source type T (dashed line), with different amplitude heights and frequencies. Here, a coarser mesh size has a damping effect, while a finer mesh resolves the wave better. The data suggests, further lowering the element size will lead to a solution with a more physical wave effect.

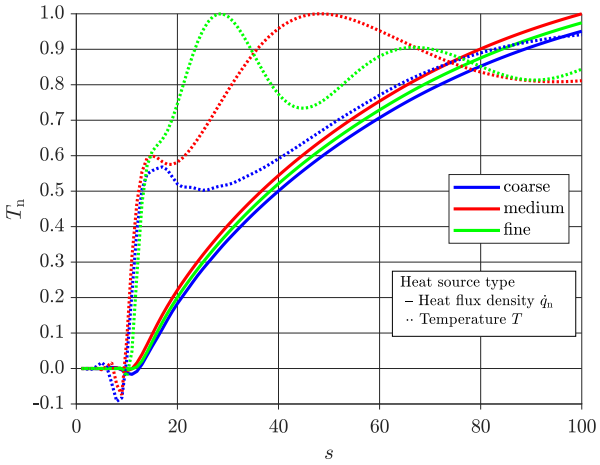

Fig. 7: T_n at $\mathrm{Ma}_\mathrm{th} = 1$ for coarse, medium and fine mesh.

5 Conclusion

The hyperbolic heat transport equation with respect to Christov-Cattaneo's formulation shows for the SUPG theory with different time integration schemes dependencies on the thermal Mach number Ma_th and the heat source type. For the subcritical diffusion no major impact is detected, while for the transcritical state the solution develops some numerical issues in space and time. Furthermore, a thermal shock in form of a steep temperature gradient is present at the leading edge of the source for $\mathrm{Ma}_\mathrm{th} = 1$. A wave behavior is only seen for a line heat source in form of a constant temperature with wiggles in the spatial and temporal solution. In addition, a finer mesh helps to counteract those problems and stabilize the wave behavior and avoids nonphysical effects. In time, the Θ method is the most stable approach, but also comes with the longest computational time. For an accurate and converging solution, and even more for the supercritical diffusion, mechanisms such as flux or slope limiters should be considered.

Acknowledgements Open access funding enabled and organized by Projekt DEAL.

References

[1] C. I. Christov, P. M. Jordan, Heat Conduction Paradox Involving Second-Sound Propagation in Moving Media (The American Physical Society, 2005)
[2] M. C. Feike, Ch. Mundt, Space-time stabilized FEM applied on the hyperbolic heat conduction equation for high speed frictional contact (Wiley, 2021)
[3] D. D. Joseph, L. Preziosi, Heat waves (The American Physical Society, 1988)
[4] G. Lebon, D. Jou, J. Casas-Vázques, Understanding Non-equilibrium Thermodynamics (Springer, 2008), chap. 7.1.1
[5] D. Y. Tzou, Shock wave formation around a moving heat source in a solid with finite speed of heat propagation (Pergamon Press, 1989)
[6] D. Y. Tzou, On the Thermal Shock Wave Induces by a Moving Heat Source (ASME, 1989)
[7] O. Nosko, Perfect thermal contact of hyperbolic conduction in semispace with an interfacial heat source (Elsevier, 2020)
[8] H. Altenbach, Kontinuumsmechanik: Einführung in die materialabhängigen und materialunabhängigen Gleichungen (Springer, 2018), chap. 5
[9] D. Y. Tzou, Macro- to microscale heat transfer (Wiley, 2015), chap. 1.5
[10] H. Gómez, I. Colominas, F. Navarrina and M. Casteleiro, A hyperbolic model for convection-diffusion transport problems in CFD: Numerical analysis and applications (RACSAM, 2008)
[11] W. Polifke, J. Kopitz, Wärmeübertragung: Grundlagen, analytische und numerische Methoden (Pearson Studium, 2009)
[12] J. Donea, A. Huerta, Finite Element Methods for Flow Problems (Wiley, 2003)
[13] K. H. Huebner, D. L. Dewhirst, D. E. Smith, T. G. Byrom, The Finite Element Method for Engineers (Wiley, 2001), chap. 7.5.3.
[14] J. Donea, L. Quartapelle, An introduction to finite element methods for transient advection problems (Elsevier, 1992)
[15] P. B. Bochev, M. D. Gunzburger, J. N. Shadid, Stability of the SUPG finite element method for transient advection–diffusion problems (Elsevier, 2004)
[16] H.-C. Huang, A. S. Usmani, Finite Element Analysis for Heat Transfer (Springer, 1994), p. 109
[17] K.-J. Bathe, E. L. Wilson, NUMERICAL METHODS IN FINITE ELEMENT ANALYSIS (Prentice-Hall, 1976), chap. 8.2
[18] Z. Zhou, Y. Wen, C. Cai, Q. Zeng, Fundamentals of Structural Dynamics (Elsevier, 2021), chap. 7

[19] S. Rostami, R. Kamgar Insight to the Newmark Implicit Time Integration Method for Solving the Wave Propagation Problems (Springer, 2021)
[20] B. Bhushan: Modern tribology handbook - Volume One - Principles of Tribology, (CRC Press, 2001)